# Dalton Transactions

Accepted Manuscript






ROYAL SOCIETY OF CHEMISTRY

www.rsc.org/dalton

Cite this: DOI: 10.1039/c0xx00000x

www.rsc.org/xxxxxx

ARTICLE TYPE

# Copper(II) Coordination Polymers: Tunable Structures and Different Activation Effect of Hydrogen Peroxide for the Degradation of Methyl Orange under Visible Light Irradiation

**Lu Liu,[a] Dongqing Wu,[a,b] Bei Zhao,[a] Xiao Han,[a] Jie Wu,*[a] Hongwei Hou*[a] and Yaoting Fan[a]**

***Received (in XXX, XXX) Xth XXXXXXXXX 20XX, Accepted Xth XXXXXXXXX 20XX***
***First published on the web Xth XXXXXXXXX 20XX***
**DOI: 10.1039/b000000x**

By tuning synthesis conditions, based on a conformation-sensitive ligand 1,4-bis(1,2,4-triazole-1-methylene)-2,3,5,6-tetramethyl benzene (btmx) and $Cu(NO_3)_2·3H_2O$/$CuCl_2·2H_2O$, we obtained three Cu(II) coordination polymers with diverse structures, namely, $\{[Cu(btmx)_2(H_2O)]·2NO_3\}_n$ **(1)**, $\{[Cu(btmx)_2(Cl)_2]·5H_2O\}_n$ (**2**) and $\{[Cu(btmx)(Cl)_2]_n$ (**3**). Complex **1** exhibits a novel 2D→3D interpenetrating structure with the point symbol of $6^3$. Complex **2** features an irregular 2D grid with $(4^4·6^2)$ topology. The structure of complex **3** is a 1D double chain structure. The ultraviolet-visible absorption spectrums and TG curves of these complexes are also presented and discussed. Moreover, under visible light, coordination polymers **1**, **2**, **3** display different activation effect of hydrogen peroxide ($H_2O_2$) for photocatalytic decomposing methyl orange (MO), which indicates that coordination polymers may have bright prospect in the field of photocatalytic degrading dyes.

## Introduction

Dye wastewater, which is mainly produced in the production of dyes and dye intermediates, has been the problem of industrial wastewater treatment for a long time due to the deep chromaticity, strong toxicity and degradation-resistant properties.[1,2] As a dye wastewater treatment, photocatalytic oxidation method, which can be performed under mild conditions and degrade organic dyes to non-toxic inorganic compounds, is a very promising technology and one of the focus of wastewater treatment.[3,4] Currently, the commonly used photocatalytic materials with excellent performance, are mainly focused on $TiO_2$, ZnO, metal titanate and niobate and other semiconductor with wide band gap. However, bandgaps of these semiconductors are usually above 3eV, resulting in the absorbtion of a small amount of ultraviolet from sunlight.[5,6]

As is well known, coordination polymers (CPs), which are constructed by multitudinous metal ions and ligands, are usually insoluble and stable in common organic solvents or aqueous solutions. These intrinsic properties thus render coordination polymers to be potentially used as green heterogeneous catalysts which could readily be reused.[7-10] Owing to the difficulties of synthesizing stable, efficient and band-gap tunable CP-based catalysts, the application of coordination polymers on visible-light driven photocatalysis degrading dyes is just beginning to emerge recently.[11-15] Theoretically, coordination polymers can be very promising as photocatalytic degradation materials, for the reason that both the metal ions and the organic moieties can provide the platforms to generate varying bandgaps, while metal−ligand coordinating interactions can regulate the bandgap widths. Furthermore, the high diversity of structures and controllable pore sizes of coordiantion polymers permit their different behaviors in photocatalytic degradation, which can also impact the degradation efficiency. The integration of high crystallinity, and tunable porosity in these coordination polymer materials should offer large interfacial surface areas, short electron–hole diffusion lengths to the internal interfaces, and

[a] *The College of Chemistry and Molecular Engineering, Zhengzhou University, Zhengzhou 450052, P. R. China* Fax: (+86) 371−67761744
[b] *State Key Laboratory of Coordination Chemistry, School of Chemistry and Chemical Engineering, Nanjing University, Nanjing 210093, China*
*E-mail: houhongw@zzu.edu.cn; wujie@zzu.edu.cn*
*†Electronic supplementary information (ESI) available: X-ray crystallographic data, selected bond lengths and bond angles, powder X-ray patterns, TGA curves for complexes **1**−**3** and UV−vis absorption of MO at different time intervals under Xe lamp irradiation. CCDC reference numbers:1009806–1009808 for **1**−**3**. For ESI and crystallographic data in CIF or other electronic format see DOI:10.1039/b000000x/*

multiple routes for band gap engineering through compositional and structural control. Thus, coordination polymers with narrow bandgaps can absorb visible light and may have broad prospects in developing new efficient visible light photocatalytic materials.

Large amounts of investigations have shown that in the process of assembling, the environments, such as pH value, solvent, temperature, and reagent concentration *etc*., have an unpredictable impact on the coordinating reaction or crystallization of coordination polymers.[16-18] Minor changes of such environmental factors may lead to different architectures originated from differences in atomic connectivity or network catenation. In this paper, we employ 1,4-bis(1,2,4-triazole-1-methylene)-2,3,5,6-tetramethyl benzene (btmx), the conformation of which is sensitive to external stimuli (temperature and solvents etc.), to construct three Cu(II) coordination polymers with diverse structures, namely, $\{[Cu(btmx)_2(H_2O)]\cdot 2NO_3\}_n$ **(1)**, $\{[Cu(btmx)_2(Cl)_2]\cdot 5H_2O\}_n$ (**2**) and $\{[Cu(btmx)(Cl)_2]_n$ (**3**). The structures of these complexes, along with the ultraviolet and visible absorption spectrum, photocatalytic degrading methyl orange (MO) by complexes **1**, **2**, **3** under visible light are presented and discussed, and the results indicate that they were capable of activating hydrogen peroxide ($H_2O_2$) in photocatalytic process.

## Experimental section

**Materials and Physical Measurements.**

All reagents and solvents were commercially available except for btmx, which was synthesized according to the literature.[19] The FT-IR spectra were recorded from KBr pellets in the range of 400–4000 $cm^{-1}$ on a Bruker Tensor 27 spectrophotometer. Elemental analyses (C, H, and N) were carried out on a FLASH EA 1112 elemental analyzer. PXRD Patterns were recorded using Cu Kα1 radiation on a PANalytical X'Pert PRO diffractometer. Thermal analyses were performed on a Netzsch STA 449C thermal analyzer from room temperature at a heating rate of 10 °C $min^{-1}$ in air. UV−Vis diffused reflectance spectra of the samples were obtained for the dry-pressed film samples using a Cary Series UV−Vis-NIR spectrophotometer. $BaSO_4$ was used as a reflectance standard in a UV–Vis diffuse reflectance experiment. UV−Vis absorption spectra of Fig.S3 were put into effect with a TU-1901 double-beam UV−Vis Spectrophotometer. The measurements of the UV−Vis absorption spectra of Fig.S4 and Fig.S6a were conducted on a Agilent 8453 single-beam UV−Vis Spectrophotometer.

**Photocatalytic Measurement.**

A photocatalytic experiment in aqueous solution was carried out. A 30 mg portion of coordination polymers and 0.5 mL of 30% $H_2O_2$ were added into the methyl orange aqueous solutions (50 mL, 18 mg/L). The mixture was stirred for half an hour in a dark environment to get a balance between adsorption and desorption. A 500 W xenon arc lamp was used as a light source. Visible light then irradiated the above solutions and it was stirred constantly. Every 20 min, we took a 5 mL sample from the reaction system and the supernatant liquid obtained by centrifugation was used for the UV−visible analysis. The characteristic peak (λ = 465 nm) for methyl orange was employed to monitor the photocatalytic decomposition process. Meanwhile, we set three sets of contrast tests, namely, adding complex only or adding 0.5 mL of 30% $H_2O_2$ only or adding $H_2O_2$ and copper(II) salts. Taking complex **2** for example, in stead of taking samples from the same reaction, the parallel reactions which provide samples at different time are also performed.

**Synthesis**

**Synthesis of $\{[Cu(btmx)_2(H_2O)]\cdot 2NO_3\}_n$ (1).** A mixture of $Cu(NO_3)_2\cdot 3H_2O$ (24.1 mg, 0.1 mmol), btmx (29.8 mg, 0.1 mmol) and 10 mL distilled $H_2O$ was sealed in a 25 mL Teflon-lined stainless steel container and heated at 130 °C for 3 days. After the mixture cooled to room temperature at a rate of 5 °C/h, needle-like green crystals of **1** were obtained with a yield of 53% (based on Cu). Anal. Calcd for $C_{32}H_{42}N_{14}O_7Cu$ (%): C, 48.14; H, 5.30; N, 24.56. Found: C, 48.35; H, 5.37; N, 24.23. IR (KBr, $cm^{-1}$): 3383(w), 3287(w), 3109(m), 3000(w), 1668(w), 1530(m), 1381(s), 1286(m), 1216(m), 1131(m), 1037(w), 1000(w), 902(w), 827(w), 768(w), 678(w), 649(w).

**Synthesis of $\{[Cu(btmx)_2(Cl)_2]\cdot 5H_2O\}_n$ (2).** A mixture of $CuCl_2\cdot 2H_2O$ (17.1 mg, 0.1 mmol), btmx (29.8 mg, 0.1 mmol) and 10mL distilled $H_2O$ was sealed in a 25 mL Teflon-lined stainless steel container and heated at 100 °C for 3 days. After the mixture cooled to room temperature at a rate of 5 °C/h, rodlike blue crystals of **2** were obtained with a yield of 60% (based on Cu). Anal. Calcd for $C_{32}H_{44}N_{12}O_2Cl_2Cu$ (%): C, 50.36; H, 5.81; N, 22.02. Found: C, 50.57; H, 5.72; N, 22.43. IR(KBr, $cm^{-1}$): 3425(w), 3130(m), 3008(w), 1739(w), 1662(w), 1623(w), 1523(w), 1400(s ), 1277(w), 1126(w), 1002(w), 883(w), 828(w), 768(w), 675(w), 646 (w).

**Synthesis of $\{[Cu(btmx)(Cl)_2]_n$ (3).** A mixture of $CuCl_2\cdot 2H_2O$ (17.1 mg, 0.1 mmol), btmx (29.8 mg, 0.1 mmol) and 8mL distilled $H_2O$, 2 mL $CH_3OH$ was sealed in a 25 mL Teflon-lined stainless steel container and heated at 100 °C for 3 days. After the mixture cooled to room temperature at a rate of 5 °C/h, green crystals of **3** were obtained with a yield of 67% (based on Cu). Anal. Calcd for $C_{16}H_{20}N_6Cl_2Cu$ (%): C, 44.61; H, 4.68; N, 19.51. Found: C, 44.91; H, 4.56; N, 19.22. IR(KBr, $cm^{-1}$): 3113(m) 2960(w), 1512(s), 1440(s), 1403(m), 1385(m), 1271(s) 1208(w), 1183(w), 1127(s), 1009(s), 986(s), 875(w), 866(w), 817(w), 751(s), 675(s), 647(w).

**Crystal Data Collection and Refinement.**

The data of **1**−**3** were collected on a Rigaku Saturn 724 charge-coupled device (CCD) diffractomer (Mo-Kα, λ= 0.71073 Å) at a temperature of 20 ± 1 °C. Absorption corrections were applied by using a multiscan program. The data were corrected for Lorentz and polarization effects. The structures were solved by direct methods and refined with a full-matrix least-squares technique based on $F^2$ with the SHELXL-97 crystallographic software package.[20] The refinement of **1** also used OLEX 2 software. The hydrogen atoms were placed at calculated positions and refined as riding atoms with isotropic displacement parameters. There are large solvent accessible void volumes in the crystal of **2** which are occupied by free water molecules. No satisfactory disorder model could be achieved, and therefore the SQUEEZE program implemented in PLATON was used to remove these electron densities.[21] The final chemical formula of **2** were calculated from

SQUEEZE results combined with the TGA and elemental analysis data. Crystallographic crystal data and structure processing parameters for **1**–**3** are summarized in Table S1 (Supporting Information). Selected bond lengths and bond angles of **1**–**3** are listed in Table S2 (Supporting Information). Crystallographic data for the structures in the form of CIF files have been deposited with the Cambridge Crystallographic Data Centre as supplementary publication Nos. CCDC 1009806–1009808 for complexes **1**–**3**, respectively.

## Results and discussion

**Crystal Structure of $\{[Cu(btmx)_2(H_2O)]\cdot 2NO_3\}_n$ (1)**

Single-crystal X-ray crystallographic analysis reveals that **1** crystallizes in the orthorhombic system, space group *Ibam*. As shown in Fig.1a, the coordination environment around the Cu(II) center can be defined as a slightly distorted $[CuN_4O]$ trigonal bipyramid geometry, which is completed by one oxygen atom (O1) from one coordinated water molecule and four nitrogen atoms (N1, N1A, N4, N4A) from four btmx ligands. The bond lengths of Cu–O and Cu–N are similar to those in other Cu(II) complexes (Cu(1)–N(1)/N(1A) = 2.032 Å, Cu(1)–N(4)/N(4A) = 2.047 Å, Cu(1)–O(1) = 2.249 Å).

Interestingly, there are two kinds of btmx ligands with different conformation in complex **1**. One is symmetric *cis*-conformation with $N_{donor}\cdots N{-}C_{sp3}\cdots C_{sp3}$ torsion angle of 49.183°. The other is symmetric *trans*-conformation with $N_{donor}\cdots N{-}C_{sp3}\cdots C_{sp3}$ torsion angle of 122.101°. Two adjacent btmx ligands of symmetric *cis*-conformation connect two Cu(II) ions to give rise to a macrocycle. The two coordinated water molecules point to the center of the ring. The Cu1···Cu1 distance is 8.571 Å within each macrocycle. Further, these macrocycles are connected by btmx ligands with symmetric *trans*-conformation to generate a 2D grid structure, as shown in Fig.1b. The vertexs of the grid are occupied by these macrocycles, with the Cu1···Cu1 distance between neighbouring two macrocycles of 15.055 Å.

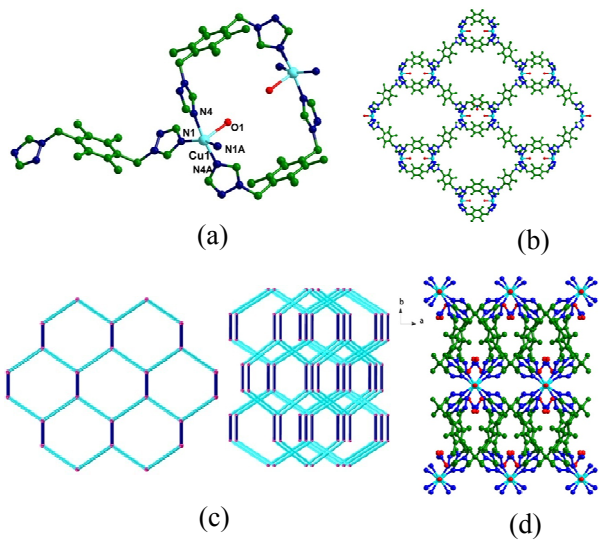


Fig. 1 (a) Coordination environment of the Cu(II) ions in **1**. Hydrogen atoms and are omitted for clarity; (b) The 2D grid structure containing macrocycles; (c) Schematic representation of the 2D→3D interpenetrating nets in **1**; (d) The top view of the 3D framework from *a* axis.

From the topological point of view, each Cu(II) ion can be defined as a three-connected node, btmx can be viewed as a linker, the simplified graphic of the 2D grid is shown in Fig.1c. The lengths of three diagonals within each hexagon are 26.738×26.738×24.856 Å. The potential voids are filled via mutual interpenetration of the other independent equivalent grids in a interlaced mode, giving rise to a 2D to 3D interpenetrating framework (Fig.1c). The top view of the 3D framework from *a* axis is shown in Fig.1d.

**Crystal Structure of $\{[Cu(btmx)_2(Cl)_2]\cdot 5H_2O\}_n$ (2)**

The X-ray crystallographic analysis reveals that complex **2** crystallizes in the monoclinic crystal system, space group *P*2(1)*/c*. As depicted in Fig.2a, the Cu(II) center adopts distorted octahedral coordination geometries, of which the six vertexes are N1, N1A, N4, N4A, Cl1, Cl1A. Among them, four nitrogen atoms come from four btmx ligands. The bond lengths are listed below: Cu(1)–N(1)/N(1A) = 2.009 Å, Cu(1)–N(4)/N(4A) = 2.021Å, Cu(1)–Cl(1)/Cl(1A) = 2.922 Å. It should be noted that, the Cu(1)–Cl(1)/Cl(1A) bond lengths are elongated owing to Jahn-Teller Effect.

Different to **1**, the two kinds of btmx ligands in **2** both present symmetric *trans*-conformation. The $N_{donor}\cdots N{-}C_{sp3}\cdots C_{sp3}$ torsion angles of btmx which contains N1 and N1A are both 120.735°. While the $N_{donor}\cdots N{-}C_{sp3}\cdots C_{sp3}$ torsion angles of btmx which contains N4 and N4A are both 130.812°. Cu(II) ions bond with btmx ligands to yield a 2D grid structure(Fig.2b). The diagonal lengths within each grid are 12.925×26.772 Å. The coordinated chlorine atoms lie above or below the 2D grid layer.

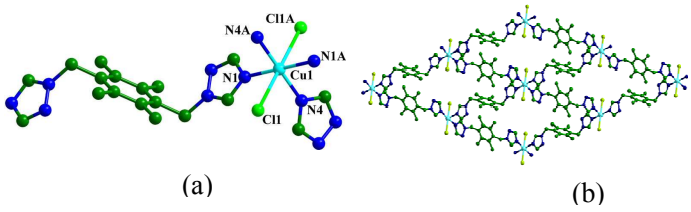


Fig. 2 (a) Coordination environment of the Cu(II) ions in **2**. Hydrogen atoms and are omitted for clarity; (b) The 2D grid structure of **2**.

**Crystal Structure of $\{[Cu(btmx)(Cl)_2]_n$ (3).**

X-ray crystallographic analysis reveals that complex **3** crystallizes in the monoclinic crystal system, space group *P*2(1)*/c*.

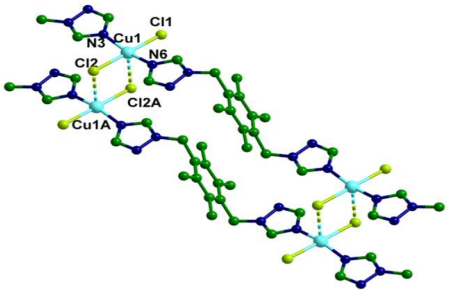


Fig. 3 1D double chain structure of **3**. Hydrogen atoms and are omitted for clarity.

As displayed in Fig.3a, the Cu(II) center adopts distorted trigonal bipyramid geometry, of which the five vertexes are N3, N6, Cl1, Cl2, Cl2A. Among them, two nitrogen atoms come from two symmetric related btmx ligands with translation operation of (-1,

0, -1). The bond lengths are listed below: Cu(1)–N(3) = 2.023 Å, Cu(1)–N(6) = 2.012Å, Cu(1)–Cl(1) = 2.253 Å, Cu(1)–Cl(2) = 2.320 Å, Cu(1)–Cl(2A) = 2.818 Å. It is noted that the Cu(1)–Cl(2A) bond length is longer than normal Cu–Cl bond owing to Jahn-Teller effect.

Different to **1** and **2**, **3** only contains one kind of btmx. Btmx adopt asymmetric *trans*-conformation and the $N_{donor}\cdots N{-}C_{sp3}\cdots C_{sp3}$ torsion angles are 115.848° and 120.853°, singly. Two adjacent 1D chains constructed by Cu(II) ions and btmx ligands are linked into 1D double chain by sharing Cl2 and Cl2A.

**PXRD Patterns and Thermal Stability.**

To estimate the stability of the coordination architectures, thermogravimetric analyses (TGA) of complexes **1**, **2**, **3** were carried out. The phase purities of the bulk samples were identified by powder X-ray diffraction (Fig. S1). Results of the TGA curves show that the three complexes possess different thermal stabilities (Fig. S2). For complex **1**, there is no weight loss until the decomposition of the framework occurs at about 200 °C. However, single-crystal X-ray crystallographic analysis reveals that there exists one coordinated water in the asymmetric unit of **1**. Generally, coordinated waters lost under 100°C. As can be seen from Fig.1a, the two coordinated water molecules point to the center of the ring. Rich hydrogen bonds (O1-H1W···N1 = 3.385, O1-H2W···O2 = 2.787, O1-H2W···N7 = 3.448 Å) in complex **1** may result in the higher water losing temperature. For **2**, a slight decrease in mass between 30-125°C (4.7% predicted and 3.9% observed) marks the expulsion of two water molecules. The other disordered water molecules in the channels could have lost before thermal analysis, this may be because the (disordered) water in the channels can be easily lost on drying, while the (ordered) water is enclosed between host molecules and held more strongly. Then the whole network collapses after 240°C. Complex **3** begins to decompose at 260 °C for there is no guest molecules observed.

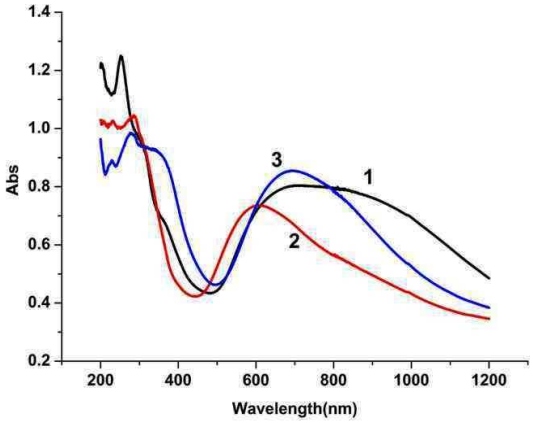


Fig.4 Solidstate ultraviolet-visible absorption spectra of complexes **1**, **2**, **3**.

**Solidstate Ultraviolet-Visible Absorption Spectrum.**

Ultraviolet-visible absorption spectrum can reflect electron transition to some extend. Here, we investigated the solidstate absorption spectra of **1**, **2**, **3** at room temperature. As shown in Fig.4, complexes **1**, **2**, **3** show different maximum absorption peaks and follow the order of **1**≈**3**>**2**. It may be attributed to the different coordination configuration that effects d-d transition energy. Complexes **1** and **3** display similar maximum absorption wavelength numbers, respectively, which may be due to similar coordination configuration. The Cu(II) ions in **1** and **3** have triangular bipyramid coordination configuration, while Cu(II) ions in **2** display octahedral coordination configuration.

**Photocatalysis Experiment.**

To explore the photocatalytic degradation behavior of complexes

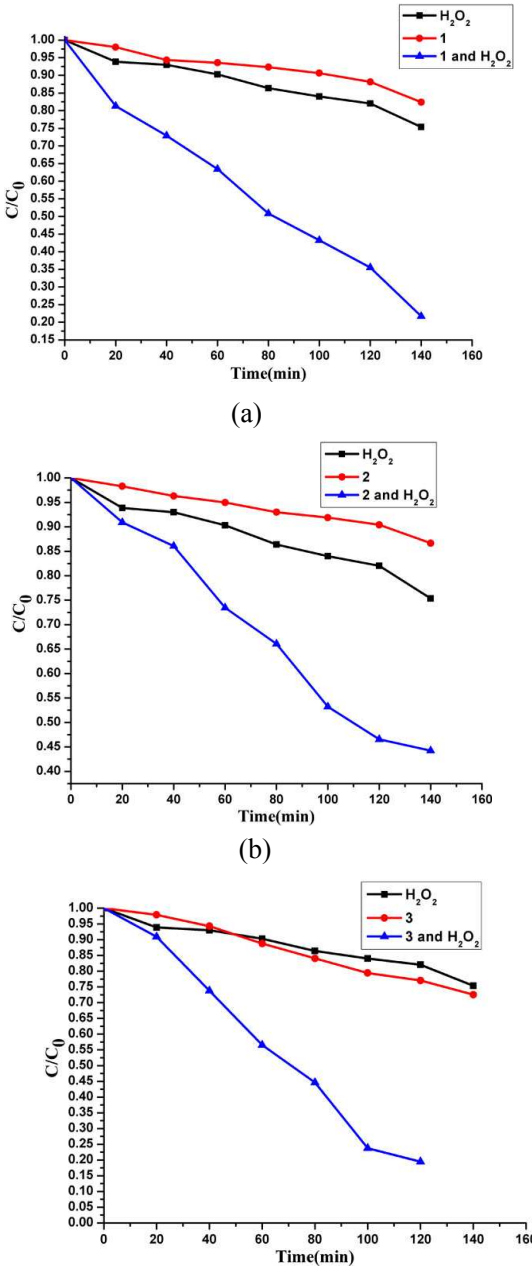


Fig. 5 Concentration changes of MO at different time intervals under Xe lamp irradiation: (a) For complex **1**; (b) For complex **2**; (c) For complex **3**.

**1**, **2**, **3**, the photocatalytic decomposition of a commonly used dye methyl orange (MO) was investigated. Complexes **1**, **2**, **3** exhibit good photocatalytic activities in the presence of $H_2O_2$ under Xe

lamp irradiation. As the photocatalytic degradation continues, the absorption peak intensity of MO gradually reduces (Fig.S3 and Fig.S4). Moreover, the concentration changes in MO aqueous solution were plotted versus irradiation time (Fig.5 and Fig.S5). The degradation rate under Xe lamp is 24% with 0.5 mL 30% $H_2O_2$ only, and is 18, 14, 27% with the presence of complex **1**, **2**, **3** only, and is 20% with the presence of $H_2O_2$ and $Cu(NO_3)_2{\cdot}3H_2O$ and 16% with $H_2O_2$ and $CuCl_2{\cdot}2H_2O$, it increases to 80, 56, 81% when adding both $H_2O_2$ and complex **1**, **2**, **3**, respectively. Besides, in stead of taking samples from the same reaction, the result of parallel reaction of complex **2** shows that 55% of the MO has been dissociated after 140 min of irradiation (Fig.S6), which is consistent with the above-mentioned result.

In general, a large maximum absorption wavelength leads to the ease of the charge separation, so the photocatalytic decomposition rate of MO should follow the order of maximum absorption wavelength of the complexes. As discussed above, the maximum absorption wavelength of complexes **1**, **2**, **3** follow the order of **1**≈**3**>**2**, which coincidently accords with the order of decomposition rate of MO. Besides, the Cu(II) ions in **1** and **3** have unsaturated triangular bipyramid coordination configuration, while Cu(II) ions in **2** display saturated octahedral coordination configuration. There is unoccupied sites on unsaturated Cu(II) centers to interact with $H_2O_2$, while it is hard for saturated Cu(II) centers to react with $H_2O_2$. Based on the above, we speculate that the activation effects of Cu(II)-CPs in photocatalytic degradation of MO occurred in two possible routes: (i) it could be catalytically decomposed by Cu(II)-CPs to produce •OH radicals through the Fenton-like reaction, where $Cu^{2+}$ reacts with $H_2O_2$ to generate hydroxyl radicals along with the reduction–oxidation cycle of Cu(II)–Cu(I);[22-24] (ii) by absorption of energy equal to or greater than the band gap of the Cu(II)-CPs, the electrons ($e^-$) are excited from the valence band (VB) to the conduction band (CB), leaving the holes (h+) in the VB. The electrons and holes migrate to the surface of the Cu(II)-CPs, then the photoinduced energy transfers to the adsorbed species: electrons reduce the oxygen ($O_2$) to oxygen radicals(•$O_2$) and finally they transform into hydroxyl radicals(•OH); in turn, holes oxidize the hydroxyl (HO-) to hydroxyl radicals (•OH) ($H_2O_2$ provides part of the $O_2$ and hydroxyl). Hydroxyl radicals (•OH) have the ability to decompose methyl orange effectively.[25,26]

Solid residues of complexes **1**, **2**, **3** which were isolated from the reaction mixture via centrifugation, displayed the same PXRD patterns as that of the original solid samples (Fig. S7). These results support that **1**, **2**, **3** have adequate stability to be used as efficient heterogeneous catalysts for the degradation of MO.

## Conclusions

Three Cu(II) coordination polymers exhibiting different activation effect of hydrogen peroxide ($H_2O_2$) under visible light were synthesized by tuning reaction condition of Cu(II)/btmx system. It demonstrates that by tuning reaction condition the coordination behavior between metal ions and ligands may change, thus leading to complexes with diverse structures and maximum absorption wavelengths. The phenomenon that coordination polymers **1**, **2**, **3** display different activation effect of hydrogen peroxide ($H_2O_2$) in photocatalytic degrading methyl orange (MO) under visible light indicates that coordination polymers may have bright prospect in the field of photocatalytic degrading dyes.

## Acknowledgments

This work was financially supported by the National Natural Science Foundation (No 21371155 and 21201152) and Research Fund for the Doctoral Program of Higher Education of China (20124101110002).

## References

1 M. R. Hoffmann , S. T. Martin , W. Choi , D. W. Bahnemann, *Chem. Rev*. 1995, **95**, 69.
2 P. Waranusantigul, P. Pokethitiyook, M. Kruatrachue, *Environ. Pollut*. 2003,**125**, 385.
3 O. Legrini, E, Oliveros, A. M. Braunm, *Chem. Rev*. 1993, **93**, 671.
4 A. Mills, R. H. Davies, D. Worsley, *Chem.Soc.Rev*. 1993, **22**, 417.
5 M. N. Chong, B. Jin, C. W. K. Chow, *Water Research*. 2010, **44**, 2997.
6 E. Piera, M. I. Tejedor-Tejedor, M. E. Zorn, M. A. Anderson, *Applied Catalysis ( B: Environmental)*. 2003, **46**, 671.
7 M. D. Allendorf, C. A. Bauer, R. K. Bhaktaa and R. J. T. Houka, *Chem. Soc. Rev*. 2009, **38**, 1330.
8 M. Kurmoo, *Chem. Soc. Rev*. 2009, **38**, 1353.
9 R. Babarao, J. W. Jiang, *J. Am. Chem. Soc*. 2009, **131**, 11417.
10 R. Feng, F. L. Jiang, L. Chen, C. F. Yan, M. Y. Wu and M. C. Hong, *Chem. Commun*. 2009, 5296.
11 T. Wen, D. X. Zhang, J. Liu, R. Lin and J. Zhang, *Chem. Commun*. 2013, **49**, 5660
12 P. Mahata, G. Madras, S. P. Natarajan, *J. Phys. Chem. B*. 2006, **110**, 13759.
13 F. Wang, Z. S. Liu, H. Yang, Y. X. Tan, J. Zhang, *Angew. Chem., Int. Ed*. 2011, **50**, 450.
14 L. L.Wen, F. Wang, J. Feng, K. L. Lv, C. G. Wang and D. F. Li, *Cryst. Growth Des*. 2009, **9**, 3581.
15 Y. L. Hou, R. W. Y. Sun, X. P. Zhou, J. H. Wang and D. Li, *Chem. Commun*. 2014, **50**, 2295.
16 (a) B. Moulton, M. J. Zaworotko, *Chem. Rev*. 2001, **101**, 1629; (b) S. M. Fang, E. C. Sañudo, M. Hu, Q. Zhang, S. T. Ma, L. R. Jia, C. Wang, J. Y. Tang, M. Du, and C. S. Liu, *Cryst. Growth Des*. 2011, **11**, 811.
17 (a) J. Tian, R. K. Motkuri, P. K. Thallapally, B. P. McGrail, *Cryst. Growth Des*. 2010, **10**, 5327; (b) L. Yang, D. R. Powell, R. P. Houser, *Dalton Trans*., 2007, 955; (c) L. Y. Xin, G. Z. Liu, X. L. Li, and L. Y. Wang, *Cryst. Growth Des*. 2012, **12**, 147.
18 (a) P. Pachfule, R. Das, P. Poddar, R. Banerjee, *Cryst. Growth Des*. 2011, **11**, 1215; (b) L. Carlucci, G. Ciani, D. M. Proserpio, S. Rizzatio, *Chem.–Eur. J*., 2002, **8**, 1519.
19 Y. J. Mu, G. Han, S. Y. Ji, H. W. Hou and Y. T. Fan, *CrystEngComm*. 2011, **13**, 5943.
20 G. M. Sheldrick, *Acta Crystallogr. Sect. A*: *Found. Crystallogr*. 2008, **64**, 112.
21 A. L. Spek, *Acta Crystallogr., Sect. A: Found. Crystallogr*. 1990, **46**, 194.
22 G. H. Cui, C. H. He, C. H. Jiao, J. C. Geng and V. A. Blatov, *CrystEngComm*, 2012, **14**, 4210.
23 B. Ahmed, E. Limem, A. Abdel-Wahab and B. Nasr, *Ind. Eng. Chem. Res*. 2011, **50**, 6673.
24 A. Corma, H. Garcia and F. X. L. Xamena, *Chem. Rev*. 2010, **110**, 4606.
25 C. Galindo, P. Jacques and A. Kalt, J. Photochem. *Photobiol*. *A*. 2000, **130**, 35.
26 J. Joseph, H. Destaillats, H. Hung and M. Hoffmann, *J. Phys. Chem. A*. 2000, **104**, 301.

**For Table of Contents Use Only**

# Copper(II) Coordination Polymers: Tunable Structures and Different Activation Effect of Hydrogen Peroxide for the Degradation of Methyl Orange under Visible Light Irradiation

**Lu Liu,[a] Dongqing Wu,[a,b] Bei Zhao,[a] Xiao Han,[a] Jie Wu,*[a] Hongwei Hou*[a] and Yaoting Fan[a]**

By tuning reaction condition of Cu(II)/btmx system, three Cu(II) coordination polymers were synthesized. **1** exhibits a novel 2D→3D interpenetrating structure. **2** features an irregular 2D grid, while **3** displays a 1D double chain structure. Under visible light, they display different activation effect of hydrogen peroxide ($H_2O_2$) in degrading methyl orange (MO).

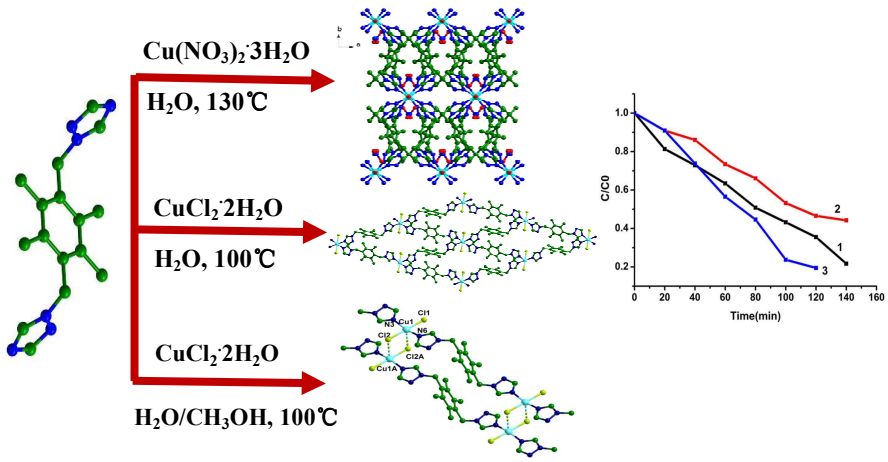

**For Table of Contents Use Only**

# Copper(II) Coordination Polymers: Tunable Structures and Different Activation Effect of Hydrogen Peroxide for the Degradation of Methyl Orange under Visible Light Irradiation

**Lu Liu,[a] Dongqing Wu,[a,b] Bei Zhao,[a] Xiao Han,[a] Jie Wu,*[a] Hongwei Hou*[a] and Yaoting Fan[a]**

By tuning reaction condition of Cu(II)/btmx system, three Cu(II) coordination polymers were synthesized. **1** exhibits a novel 2D→3D interpenetrating structure. **2** features an irregular 2D grid, while **3** displays a 1D double chain structure. Under visible light, they display different activation effect of hydrogen peroxide ($H_2O_2$) in degrading methyl orange (MO).